Epigenetic alterations underlie airway macrophage differentiation and phenotype during lung fibrosis.

Peter McErlean[1], Christopher G. Bell[2], Richard J. Hewitt[1,3], Zabreen Busharat[1], Patricia P. Ogger[1], Poonam Ghai[1], Gesa Albers[1], Shaun Kingston[3], Philip L. Molyneaux[1,3], Stephan Beck[4], Clare M. Lloyd[1], Toby M. Maher[1,3,5*‡], Adam J Byrne[1*]

[1]Inflammation, Repair and Development Section, National Heart and Lung Institute, Imperial College, London SW7 2AZ, UK.

[2]William Harvey Research Institute, Barts & The London School of Medicine, Queen Mary University of London, Charterhouse Square, London EC1M 6BQ, UK

[3]National Institute for Health Research (NIHR) Respiratory Biomedical Research Unit, Royal Brompton Hospital, Sydney Street, London SW3 6NP, UK.

[4]Department of Cancer Biology, UCL Cancer Institute, University College London, Paul O'Gorman Building, 72 Huntley Street, London WC1E 6BT, UK.

[5]Hastings Centre for Pulmonary Research and Division of Pulmonary, Critical Care and Sleep Medicine, Keck School of Medicine, University of Southern California, Los Angeles, USA.

[‡]Correspondence: t.maher@imperial.ac.uk

*Authors contributed equally

Acknowledgments:

The authors would like to acknowledge the support of the Imperial College South Kensington flow cytometry facility, particularly Ms. Jane Srivastava and Dr. Jessica Rowley. We wish to thank Dr Mark Kristiansen and Gaganjit Kaur Madhan at University College London Genomics for processing EPIC arrays. We thank Dr Michael Scherer at Department of Genetics/Epigenetics, Saarland University, Germany for advice with RnBeads analysis and providing additional code.

Funding:

P.McErlean is the recipient of the NHLI Pilot Award. A.J. Byrne is supported by a Joan Bending, Evelyn Bending, Mervyn Stephens and Olive Stephens Memorial Fellowship (AUK-SNF-2017-381). T.M. Maher is supported by a National Institute for Health Research Clinician Scientist Fellowship (ref. CS-2013-13-017) and a British Lung Foundation Chair in Respiratory Research (C17-3). C.M. Lloyd is a Wellcome Trust Senior Fellow in Basic Biomedical Science (107059/Z/15/Z**).**

Author contributions:

P. McErlean, A.J. Byrne, C.M. Lloyd and T.M. Maher designed the study. R.J. Hewitt, P.L. Molyneaux, and T.M. Maher consented patients and carried out bronchoscopies. P.P. Ogger, P. Ghai, S. Kingston, G. Albers and P.McErlean processed samples and gene expression analysis. P.McErlean, C.G.Bell, Z.Busharat and S.Beck analysed and interpreted DNA methylation data. All authors were involved in the interpretation of the results and drafting and/or revising the manuscript, provided final approval, and vouch for the content of the final manuscript.

Keywords:

Pathogenesis

Monocytes

Epigenetics

DNA methylation

Interstitial lung disease

Abbreviations:

AMs – Airway macrophages

CpG – Cytosine-guanine dinucleotides

FVC – Forced vital capacity

HC – Healthy control

DHS - DNase-I hypersensitivity sites

DNAm – DNA methylation

DMPs – Differentially methylated positions

DMRs – Differentially methylated regions

IPF - Idiopathic pulmonary fibrosis

Myld-CpGs – Myeloid marker CpG dinucleotides

pcHiC - Promoter capture HiC

scRNA-Seq - Single-cell RNA sequencing

WGBS - Whole genome bisulphite sequencing

Abstract (150 words):

Airway macrophages (AMs) are key regulators of the lung environment and are implicated in the pathogenesis of idiopathic pulmonary fibrosis (IPF), a fatal respiratory disease with no cure. However, the epigenetics of AMs development and function in IPF are limited. Here, we characterised the DNA-methylation (DNAm) profile of AMs from IPF (n=30) and healthy (n=14) donors. Our analysis revealed epigenetic heterogeneity was a key characteristic of IPF AMs. DNAm 'clock' analysis indicated epigenetic alterations in IPF-AMs was not associated with accelerated ageing. In differential DNAm analysis, we identified numerous differentially methylated positions (DMPs, n=11) and regions (DMRs, n=49) between healthy and IPF AMs respectively. DMPs and DMRs encompassed genes involved in lipid (*LPCAT1*) and glucose (*PFKB3*) metabolism and importantly, DNAm status was associated with disease severity in IPF. Collectively, our data identify that profound changes in the epigenome underpin the development and function of AMs in the IPF lung.

Background:

Airway macrophages (AMs) are sentinel innate cells of the lungs contributing to homeostasis and immune response[1]. Ontogeny of AMs is complex encompassing both self-renewing-fetal-derived 'resident' and monocyte-derived 'recruited' cells[2]. Understanding of AM ontogeny in disease states and aging is contentious and has relied heavily on murine models. However, we recently helped clarify AM ontogeny in humans by identifying that one year post lung transplant, AMs in adults are derived exclusively from recruited peripheral monocytes[3].

The influence of the local microenvironment in shaping macrophage development and function is increasingly being appreciated[4]. Responses to growth factors or inflammatory mediators can skew macrophage development as exemplified by the pro-inflammatory 'M1' and pro-wound healing 'M2' paradigm. However, *in vivo* macrophages exhibit tremendous heterogeneity in both health and diseased states[5-7], indicating a remarkable plasticity.

Key processes in macrophage development are reflected in changes to the epigenome including DNA methylation (DNAm)[8]. Occurring in the context of cytosine-guanine dinucleotides (CpGs), DNAm influences chromatin accessibility, transcription factor (TF) binding and gene expression[9,10]. DNAm represents one of the most stable epigenetic marks and can be measured as a means of assessing the influence of development and diseases on the epigenome. In AMs, DNAm is altered in genetic and environmentally-induced chronic airway diseases[11-13]. Regional differences in lung anatomy also influence DNAm in AMs[14], suggesting that shaping of AM development in the lung microenvironment comprises an epigenetic component. However, despite recent advances in our understanding of AM

ontogeny, the epigenetics of monocyte to macrophage development in the lung and influence of disease on these processes remain limited.

Idiopathic pulmonary fibrosis (IPF) is a deadly respiratory disease of unknown aetiology with heterogeneous cellular and molecular mechanisms[15]. The pathobiology of IPF is characterised by a pro-fibrotic wound-healing cascade that does not resolve, leading to progressive scarring, loss of lung function and ultimately death[16]. Although containing a strong genetic component[17], the greatest risk factor for IPF is age (median 65 years[18]) and prognosis in IPF is worse than some cancers with a mean survival of 3-5 years[19]. In the IPF lung, AMs exhibit transcriptional[7], immuno-phenotypic[1] and metabolic differences[20,21]. Recent studies employing single-cell RNA sequencing (scRNA-Seq) have indicated a transcriptional spectrum of AMs in the IPF lung that reflects facets of both M1 and M2 macrophage paradigm[5-7]. However, despite their emerging role in IPF pathogenesis, the molecular mechanisms underlying transcriptional and other phenotypic characteristics of AMs in IPF are poorly understood.

In the current study we investigated the epigenetics of AMs by undertaking genome-wide DNAm profiling using the Illumina EPIC (850k) arrays. By comparing AMs and other myeloid cell DNA methylomes, we sought to clarify the epigenetics of AM development in the lung. By profiling AMs from healthy and IPF donors, we also sought to determine if changes in the epigenome characterize features of AMs observed in the IPF lung.

Results:

The DNA methylation profile of AMs is distinct from that of peripheral monocytes or cultured macrophages:

Given recent work identifying AMs as monocyte-derived and having characteristics spanning the M1-M2 spectrum of activation, we sought to determine if these changes are also reflected at the epigenetic level by comparing the DNA methylome in AMs and other myeloid cells.

Firstly, we enriched CD206+ AMs, obtained through bronchoalveolar lavage, from healthy (n=14) and IPF (n=30) donors and assayed DNAm using Illumina Methylation EPIC (850k) arrays, which interrogate >850,000 CpGs across the genome with an enrichment for functional loci (promoters and enhancers, Table S1)[22]. These data were then merged with whole genome bisulphite sequencing (WGBS) Blueprint datasets from representative myeloid cell-types including CD14+CD16- 'Classical' and CD14+CD16+ 'Other' monocytes and *in vitro*-derived M0, M1, and M2 macrophages[23] (Figure 1A). We then identified the top 500 CpGs with a DNAm profile which best discriminated each monocyte and macrophage subtype (see methods) and characterized these as 'myeloid marker CpGs' (myld-CpGs, Table S2).

We found that myld-CpGs reside predominately in intronic and intergenic regions (Figure 1B) that are enriched for other epigenetic features in myeloid cells including histone modifications indicative of poised enhancers (H3K4me1 without H3K27ac) and open chromatin (DNase-I hypersensitivity sites: DHS, Figure 1C-D). Functional enrichment analysis additionally indicated that myld-CpGs encompass a diverse range of receptor signalling, immune cell activation, chemokine and metabolic-related processes and pathways (Figure 1E). Although annotated to n=449 genes,

158 we found AT-Rich Interaction Domain 5B (*ARID5B*), a transcriptional co factor which
159 has been shown to regulate glucose metabolism[24], contained the most myld-CpGs
160 (Figure 1F, Table S2)
161 We focused further on *ARID5B* and mining scRNA-Seq datasets from healthy and
162 diseased lung (IPF/COPD) established that *ARID5B* is expressed across immune
163 cells including monocytes and macrophages (Figure S1B). At the *ARID5B* locus we
164 found that the myld-CpGs are clustered at the promoter region of a shorter transcript
165 variant 2 and overlap with DHS and H3K4me1 enrichment (Figure 1G). We then
166 confirmed the expression of the shorter *ARID5B* transcript in AMs (Figure S1C).
167 Finally, closer inspection revealed dramatic changes in DNAm towards the shorter
168 *ARID5B* variant promoter region with AMs exhibiting an intermediate DNAm profile
169 (avg. 50.8%) compared to other myeloid cells (monocytes - avg. 85.4% and
170 macrophages - avg. 0.6%, Table S2). Taken together, these results indicate that the
171 DNAm profile of human AMs is distinct from that of peripheral monocytes/cultured
172 macrophages and we identify *ARID5B* DNAm status as a marker of AM
173 development.
174
175 **Changes in the AM-methylome define IPF-AMs:**
176 Next, to determine whether the methylome was distinct in each cell-type or disease
177 state, we clustered DNAm profiles for genes with >2 myld-CpGs. Interestingly, our
178 analysis indicated that epigenetic heterogeneity is a feature of IPF, as DNAm profiles
179 across myld-CpGs were distinct when comparing healthy and IPF AMs (Figure S1A).
180 Furthermore, the DNAm of AMs overlapped significantly with other myeloid cells,
181 potentially indicating monocytic origin (Figure S1A).

To clarify this further we performed deconvolution analysis of AM DNAm datasets with mlyd-CpGs (see methods). Deconvolution revealed that while at the epigenetic level healthy and IPF AMs were predicted to be largely a composite of 'other' monocytes and M0/M2 macrophages, clustering identified the separation of healthy and IPF AMs (Figure 2A), driven largely by differences in the minor classical monocyte and M1 macrophage fractions (Figure 2B). However, further investigation revealed that the specific differences in subsets was related to donor age (Figures 2C).

Because IPF and ageing are linked and many age-related diseases exhibit 'accelerated' changes to the epigenome, we next used DNAm 'clock' analyses to clarify the contribution of ageing towards the predicted myeloid cell composition of AMs. Epigenetic 'clocks' use changes in DNAm to estimate sample donor age and determine if accelerated epigenetic ageing are present (i.e. older age prediction than chronological age) and if disease status is associated with accelerated epigenetic signatures (see Methods). We found that while a strong correlation between chronological and epigenetic age was present, no differences in age-adjusted epigenetic age acceleration was observed between healthy and IPF AMs across either the blood or tissue-derived Hannum and Horvath 'clocks' respectively (Figure 2D and S1D). Furthermore, there was no relationship between predicted myeloid cell composition and epigenetic age acceleration (Figure 2E), inferring that myeloid cell composition was a feature of IPF AMs and not the more generalised age-related changes detected by these 'clocks'. Taken together, these data indicate that epigenetic heterogeneity is present in AMs and is a characteristic of IPF.

Identification of differentially methylated positions (DMPs) in IPF:

We next sought to determine whether AMs DNAm profiles are impacted during IPF and to identify the impact of myeloid cell composition in these analyses. Initial principal component analysis indicated a separation of donors by disease group (Figure S2A) with myeloid cell composition and donor age being comparable drivers of variance within the dataset (Figure S2D). We then undertook analysis to identify DMPs in IPF and observed a dramatic impact when adjusting for myeloid cell composition in addition to other study covariates (Figure 3A and methods). This was equally evident when investigating direction of DNAm change in IPF with all myeloid-adjusted DMPs identified (n= 11) losing DNAm compared to healthy controls (Figures 3B, S2C-D and Table S3).

IPF DMPs were either intronic (n=9) or intergenic (n=2) and occurred in regions enriched for open chromatin in myeloid cells (DHS, Figure S2E). We found n=3 IPF DMPs clustered at Lysophosphatidylcholine Acyltransferase-1 (*LPACT1*), an enzyme which mediates the conversion of lysophosphatidylcholine to phosphatidylcholine[25] (Figure 3B). Mining of scRNA-Seq data indicates that *LPCAT1* is expressed across monocytes and macrophages in the lung and we confirmed these findings in our study AMs (Figure S1B-C).

Although *LPCAT1* DMPs are intronic, distal regions can influence gene expression through 3D interactions. To investigate this further, we used promoter capture HiC (pcHiC) data to investigate the relationship between IPF DMPs and 3D interactions in myeloid cells[26]. Remarkably, while the *LPCAT1* promoter interacted with other genes/regions specifically in monocytes (Figure S2F), the strongest interaction occurred with the region containing the IPF DMPs (Figure 3C). We identified a correlation between IPF DMPs methylation and gene expression occurred only for *LPCAT1* (Figure 3D) and not any other interacting genes (Figure S2G).

Finally, we investigated the relationship between *LPCAT1* and clinical features of IPF (Table S1) and found that while no relationship was present for gene expression (Figure 3E), there was a strong correlation between methylation and forced vital capacity (FVC), a measure of disease severity and progression in IPF[27] was evident (Figure 3F). Taken together these data suggest AMs similarity to monocytes on the epigenetic and higher order 3D-interaction level and a function of DNAm of AMs in IPF pathogenesis.

Identification of differentially methylated regions (DMRs) in IPF:

Given the clustering of IPF DMPs, we next conducted analysis to identify DMRs in IPF. Similar to DMP analysis, we saw a reduction in total DMRs identified after adjusting for myeloid cell composition (Figure 4A). However, we found n=49 myeloid-adjusted DMRs which included regions both gaining and losing DNAm compared to healthy controls (Table S4). We also found n=2 DMRs which encompassed the previously identified DMPs of *LPCAT1* and DNA Polymerase Epsilon, Catalytic Subunit (*POLE*, Figure 3B).

IPF DMRs were distributed across various genomic features including promoters, introns and exons (Figure 4B), occurred in regions enriched for open chromatin in myeloid cells (Figures 4C-D) and were more likely linked in 3D to distal genes and regions (Figure S3A-C). We additionally found motifs matching TF's previously implicated in macrophage polarisation to be enriched in IPF DMRs (e.g. KLF4, FOXO1, Figure 4E) and the subsequent cell-type expression profiles of TF encoding genes across lung immune cells (Figure S3D).

We then undertook functional enrichment analysis and found enrichment across various processes and pathways pertinent to macrophage biology (e.g.

extravasations) and IPF pathogenesis (e.g. platelet activation, response to wound healing; Figure S4A).

To gain a better insight into the biological implications of changes in DNAm, we undertook additional protein-protein interaction analysis and found that DMR-associated genes form central hubs in a large interconnect network (Figure 5A and Figure S4B). We refined our analysis further and undertook functional enrichment of networks by DNAm status and found hub genes gaining DNAm in IPF predominately encompass metabolic processes whilst those losing DNAm play a role in processes and pathways pertinent to macrophage biology and fibrogenesis (e.g. phagocytosis, cell proliferation and TGF-β signalling, Figure 5B).

Given that work from our lab has identified an altered state of AM metabolism in IPF[20,21], we focused on 6-Phosphofructo-2-Kinase/Fructose-2,6-Biphosphatase 3 (*PFKB3*) , a potent driver of glycolysis[28] and found the IPF related DMR overlapped H3K4me1 and DHS enrichment and was located in an intergenic region, upstream of the *PFKB3* promoter. Remarkably, all AMs exhibited a complete loss of methylation for CpGs at the *PFKB3* TSS (Figure 5C). We found *PFKB3* exhibited differential expression between healthy and IPF AMs (Figure S1C) and subsequently confirmed a correlation between DNAm and gene expression for two of the 3 CpGs encompassing the *PFKB3* DMR (Figure 5D). We additionally identified relationships between *PFKB3* gene expression and methylation with severity of IPF as determined by FVC (Figure 5E-F). Taken together these data strongly suggest that changes in the epigenome underpin the distinct metabolic phenotype observed in AMs isolated from IPF lung and their contribution towards disease pathogenesis.

Discussion:

AMs are key regulators of the lung environment and are implicated in the pathogenesis of lung fibrosis. By comparison to reference myeloid cells, we determined that epigenetic heterogeneity is present in AMs and, furthermore, is a characteristic of IPF (Figure 2). While identified computationally, our findings mirror scRNA-Seq studies of the IPF lung where AMs exhibit transcriptional heterogeneity[5-7]. Differences in myeloid cell composition also suggests that the IPF lung influences monocyte to macrophage developmental trajectories. Interestingly, transcriptomic signatures reflective of blood monocytes are already altered in association with IPF severity[29-31], potentially indicating that the effects of IPF extends across tissue compartments rather than being isolated to the lung. As such, blood monocytes from individuals with IPF may already be 'primed' towards a particular macrophage lineage (e.g. M1-like). With advancements in single-cell epigenomics, future studies of IPF should seek to generate matched transcriptome and epigenomic datasets across blood and lung to comprehensively address the molecular events and influence of IPF on AM developmental trajectories.

In the absence of single-cell data, computational deconvolution of epigenetic data is essential to decipher disease effects within samples consisting of mixed cell populations[32]. Even though we had enriched AMs based on cell surface expression of CD206, we identified epigenetic heterogeneity (Figure 2A) and found a tremendous impact of myeloid cell composition in identification of DMPs and DMRs in IPF (Figure 3B and Figure 4A). Our work has implications for previous studies of DNAm in IPF that have largely assayed whole lung tissue in 'bulk' without accounting for cell-type heterogeneity[33,34]. Furthermore, our study employed a genome-wide

304 approach, providing better insights into the influence of IPF on the wider epigenome
305 than previously conducted gene-specific studies in this disease area [35].
306 While the identification of epigenetic heterogeneity in AMs was important for
307 deciphering DNAm changes in IPF, we additionally found that donor age correlated
308 with this predicted heterogeneity (Figure 2C). To address the potential interaction of
309 heterogeneity and age, we conducted epigenetic 'clock' analysis as these signatures
310 are actively being explored for possible novel age-related disease insights[36].
311 However, we found no differences in age acceleration between healthy and IPF AMs
312 or relationship to predicted myeloid cell composition (Figure 2D-E). These findings
313 are in contrast to many other age-related diseases[37] and indicate that whilst IPF
314 predominately occurs in later decades, the DNAm changes detected are likely to be
315 specific to IPF rather than representing epigenome changes occurring as a
316 consequence of otherwise 'healthy ageing'[38]. Although these analyses and other
317 adjustments for donor age in differential analysis revealed influence of IPF on AMs
318 DNAm, IPF and age remain inexplicably linked. Future studies of epigenetics in IPF
319 should therefore strive to include age and sex matched healthy controls.
320
321 By attempting to clarify the epigenetic events related to macrophage development in
322 the lung, we found that DNAm patterns which discriminate myeloid cell-type occur
323 largely in intronic and intergenic regions (Figure 1B). This supports previous work
324 indicating epigenomic changes during immune cell lineage commitment occurs
325 within non-coding regions[39]. However, we identified DNAm intragenically within
326 *ARID5B* at the promoter locus for a shorter transcript variant 2 as a mark of
327 monocyte to macrophage development (Figure 2G). *ARID5B* is a chromatin modifier
328 that acts as a transcriptional coactivator by removing repressive histone

329 modifications[40]. Additionally, *ARID5B* has been linked to adipogenesis[41] and
330 metabolism in hepatocytes[42] and natural killers cells, where altered DNAm
331 particularly of the short transcript variant 2 characterized a HMCV+ adaptive NK cell
332 substype[43]. More relevant to this study was work using a multi-omics approach that
333 identified *ARID5B*'s association with atherosclerosis in CD14+ blood monocytes and
334 implicated 3D interactions in linking intronic *ARID5B* DNAm (and other regulatory
335 regions) with the *ARID5B* promoter[44].
336 We identified n=11 EWAS DMPs in IPF and found most changes were clustered
337 within an intronic region of *LPCAT1* (Figure 3C). *LPCAT1* is an evolutionarily
338 conserved enzyme that is involved in phospholipid metabolism and performs a key
339 role in surfactant production in alveolar type 2 cells[45] and inflation of lungs upon
340 birth[46]. Recent work has implicated *LPCAT1* with aberrant metabolism and plasma
341 membrane remodelling in cancer, helping to establish functional links between
342 genetic alterations and tumour growth[47]. In IPF, reduction of *LPCAT1* gene
343 expression was shown to characterise subsets of IPF-specific airway epithelial
344 cells[48].
345 Similar to work in blood monocytes[44], we investigated whether integrating 3D
346 interactions could help elucidate the potential impact of changes in DNAm on gene
347 expression[26]. Remarkably, we found the *LPCAT1* promoter 'self-interacted' with
348 regions containing IPF DMPs (Figure 3C) and over half of all DMRs were linked in
349 3D to other genomic regions in myeloid cells (Figure S3C). While these data suggest
350 that similar to DNAm, AMs share a higher order chromatin structure similar to
351 monocytes and macrophages, bias from the EPIC array design needs to be taken
352 into consideration. Future studies should therefore aim to determine 3D interactions
353 in AMs from healthy and IPF donors empirically.

354 Work from our lab has indicated the crucial role of immunometabolism of AMs in
355 IPF[20,21]. We identified IPF DMRs encompassed genes and networks of lipid, iron and
356 glycolytic metabolic processes (Figure 5B and S4A-B). Indicative of the impact of
357 changes in DNAm was the DMR located at *PFKFB3* (Figure 3C), an enzyme
358 responsible for the synthesis and degradation of fructose 2,6-bisphosphate, a key
359 regulator of glycolysis. In macrophages, work has identified an important role of
360 *PFKFB3* with plasticity and the M1-phenotype in liver fibrosis[49] and with HIF-1α in
361 driving glycolytic flux and maintaining cell viability under hypoxic and inflammatory
362 conditions[50]. Given the composition of AMs in IPF was more 'M1-like' (Figure 2B)
363 and the progressive remodelling of the IPF lung results in an inflammatory hypoxic
364 environment, these results raise the question of whether development and
365 epigenetic changes identified in IPF AMs are a cause or consequence of the fibrotic
366 milieu of the IPF lung.
367
368 In conclusion, our study has identified a role of aberrant epigenetic regulation of
369 AMs, independent of ageing alone, which appears to be involved in IPF
370 pathogenesis. Our study provides a foundation for further investigations to clarify the
371 role of epigenetics during monocyte to macrophage development in the healthy and
372 diseased airways. Furthermore, our data highlight the possibility that therapeutic
373 agents targeting epigenetic modification may have a role in the treatment of IPF.
374

Methods:

Patient recruitment and sample collection:

Study donors underwent bronchoscopy and collection of BAL as outlined previously[20,21]. All study donors provided written informed consent to participate in the study, which was approved by the research ethics committee (10/HO720/12, 15/LO1399 and 15/SC/0101). Clinical characteristics of donors are outlined in Table S1. Differences in donor data were determined by Mann-Whitey or Chi-square Test for quantitative and categorical data respectively using GraphPad Prism v.8.4.2.

AMs enrichment:

CD206+ AMs were enriched from donor BAL using the magnetic-based MACS® system (Miltenyi Biotech, Germany) and fluorescent activated cells sorting (FACS) as outlined previously[3,20,21]. Briefly, for MACS-based enrichment, BAL cells (1×10^7) were incubated with human Fc-block (BD Biosciences, USA) and human CD206 APC-Cy7 (clone 15-2, BioLegend, USA). CD206+ cells were enriched in MACS LS magnetic separation column and MidiMACS^{TM} magnet. Cell counts were determined using a haemocytometer and trypan blue live/dead exclusion.

For FACS-based enrichment BAL cells were washed and incubated with near-infrared fixable live/dead stain (Life Technologies Inc.) as per the manufacturer's instructions. After incubation with human Fc block (BD Pharmingen, Inc.), surface staining was performed with the following antibodies (fluorophore followed by clone in parentheses); CD45 (PE-Texas Red, H130), CD3 (FITC, OKT), TCR- β (BV421, IP26), CD206 (PercpCy5.5, 15.2). Cell sorting was carried out on Aria III (BD Biosciences) and AMs defined as live, $CD45^+CD3^-TCR^-CD206^+$ cells.

DNA/RNA extraction and EPIC methylation arrays:

Nucleic acids were extracted from cells using the AllPrep Mini Kit (QIAGEN, Germany). DNA quality and quantity were assessed using Genomic DNA ScreenTape and TapeStation System (Agilent, USA). DNA was submitted to the UCL Genomics Core facility where bisulphite conversion, hybridization and scanning of Infinium MethylationEPIC BeadChip Arrays (Illumina, USA) were performed according to Illumina recommendations.

Array QC and pre-processing:

We employed RnBeads 2.0 pipeline[51] for methylation array preprocessing. Briefly, quality control (QC) metrics were generated and samples passing QC (e.g. bisulphite conversion efficiency) were pre-processed to remove probes with a detection P value <0.01, directly overlapping SNPs, those with SNPs within 3nt of the 3'end, cross-reactive with multiple locations and those located on sex chromosomes[52]. Processed data was then normalized using the *Dasen* function implemented from the wateRmelon package[53]. Following QC and pre-processing, 784,669 probes for each n=44 samples remained for downstream analysis.

Myeloid marker CpGs and deconvolution analysis:

Whole genome bisulphite sequencing (WGBS) data for Blueprint methylomes (2016 release)[23] were accessed through the RnBeads methylome resource (https://rnbeads.org/methylomes.html). Samples representing the myeloid cell compartment (venous blood monocytes and macrophages) and derived from donors of age comparable to our study population (i.e. >50 years) were selected (Table S5) and WGBS data pre-processed through the RnBeads pipeline as outlined above.

EPIC array and WGBS data were then merged (custom scripts available upon request) resulting in 298,945 CpGs across each n=44 CD206+ and n=13 reference methylomes. The top 500 most variable CpGs were then used to identify 'myeloid-marker CpGs' and subsequently deconvolute and predict myeloid cell composition of AMs using the Houseman method[54] implemented in RnBeads. Heatmaps were produced using Morpheus (https://software.broadinstitute.org/morpheus).

Differential methylation:

DMP analysis was performed using the meffil R pipeline[55] which implements standard and rigorous Illumina DNA methylation array QC, normalisation and subsequently Epigenome-wide Association Study (EWAS) analysis. In addition to preprocessing outline above, standard meffil QC parameters were employed to detect poor probes and/or samples for removal. Zero outliers were detected based on deviations from mean values for control probes and 6 Principal Components (PCs) were assessed to be needed to adjust for technical effects.

In total four IPF Vs Healthy EWAS were run: (i) No adjustment for covariates (ii) adjustments for 'All' covariates: age, sex, smoking history, FACS/MACS enrichment; (iii) adjustments for 'All + myeloid composition': age, sex, smoking history, FACS/MACS enrichment with addition of predicted monocyte and M0, M1, M2 macrophage composition and (iii) - as outlined for (ii) but Phenotype randomised retaining all other covariate information consistent (data not shown). Quantile-quantile (QQ) plots were generated and inspected for EWAS QC and p-value inflation. A robust genome-wide significance threshold of P value < $9x10^{-8}$ as detailed by Mansell et al.[56] was employed to identify significant DMPs.

DMRs were identified using DMRcate[57] after covariate adjustments outlined above. DMRs contained >3 CpGs and were ranked based on min-smoothed false discovery rate (FDR P<0.05).

Genomic and epigenomic feature enrichment:

Genomic feature distribution and annotation of myeloid marker CpGs, DMPs, DMRs and all EPIC probes were identified using HOMER[58] (*annotatePeaks.pl*). Enrichment across epigenomic features from monocytes and macrophages derived from Blueprint consortia were conducted with eForge 2.0[59] and EpiAnnotator[60]. For Epiannotator analysis, genomic coordinates were firstly converted from hg19 to hg38 using the *CrossMap BED* tool implemented in Galaxy Europe sever[61].

H3K4me1 ChIP-Seq data was accessed through the International Human Epigenomics Consortium portal (https://epigenomesportal.ca/ihec/grid.html). All Blueprint H3K4me1 datatracks for 'monocytes', 'CD14-positive, CD16-negative classical monocyte', 'macrophage', 'inflammatory macrophages' and 'alternatively activated macrophage' were exported and merged in the UCSC genome browser. Additional DNase-seq data was obtained for 'monocytes' and 'macrophages' using ChIP-Atlas[62].

3D interactions:

Promoter capture Hi-C (pcHiC)[26] was used to investigate relationships between differential DNAm and 3D architecture. pcHi-C data was accessed (https://osf.io/u8tzp/files/) and overlapped with DMPs and DMRs using bedtools. To address the potential biasing of promoter-based capture and prominence of

CpGs/EPIC probes at gene promoters, we selected only 'other-end' (OE's) interactions overlapping DMPs/DMRs. Unique 'baits' of overlapping OE's with interactions >5 in monocytes and macrophages where subsequently used to identify genes linked in 3D to differential DNAm. Enrichment of overlap was determined using Chi-square test with Yates correction using GraphPad Prism v.8.4.2..

Functional enrichment:

Gene ontology processes and KEGG pathway enrichment of DMR-associated genes was conducted using *goregion* function implemented in DMRcate. Additional protein-protein interaction networks and functional enrichment were identified using NetworkAnalyst 3.0[63] and the IMEx Interactome database.

Epigenetic clock analysis:

The minfi R package[64] was used to extract array data and the recommended probe-type normalization for clock analysis was performed (preprocess = Noob). A subset of the 30,084 CpGs were extracted from the total array probe set using the datMiniAnnotation3.csv file for Advanced Analysis utilising the DNAm age calculator (https://dnamage.genetics.ucla.edu)[65]. Due to differences in the 850k array, 2,552 CpGs are not included in this list. A sample annotation file including donor chronological age, sex, and tissue type was also included. Age-adjusted epigenetic age acceleration across the major blood cell-type-derived Hannum[66] and pan tissue-Horvath[65] clocks was calculated for each donor (n=44 total) and subsequently compared between IPF and healthy donors and myeloid cell composition. P values were determined via Mann-Whitney Test using GraphPad Prism v.8.4.2.

Motif Enrichment:

HOMER was used to conduct motif enrichment in DMRs (*findMotifsGenome.pl -size given*). For known motifs the HOCOMOCO v11 database was used[67]

Diseased lung scRNA-Seq data mining:

We accessed lung immune cell scRNA-Seq data via the IPF Cell Atlas (www.ipfcellatlas.com) and utilized the Kaminski/Rosas dataset which includes samples from healthy controls and donors with IPF and COPD[5].

Quantitative real-time PCR (qPCR):

Gene expression was performed as outlined previously[20,21]. Taqman probes used in this study were purchased from Thermo scientific: *LPCAT1* (Hs00227357_m1), *SLC12A7* (Hs00986431_m1), *SLC6A3* (Hs00997374_m1), *ARID5B* (Hs01382781_m1), *PFKFB3* (Hs00998698_m1). Spearman rank correlations between differential DNAm, clinical variables and expression were identified using GraphPad Prism v.8.4.2.

Data availability:

All EPIC methylation array data has been deposited on Gene Expression Omnibus (GSE159655).

Figures 1:

(A) Outline of approach to investigate relationship between airway macrophages (AMs) and other myeloid cell-types (i.e. monocytes and macrophages) DNA methylation (DNAm) as determined by EPIC and whole genome bisulphite sequencing (WGBS) respectively. Cell-type depictions were generated using www.biorender.com.

(B) Genomic feature distribution for merged AMs and myeloid cell DNAm datasets and the n=500 myeloid marker CpGs to be used in deconvolution analysis.

(C-D) Enrichment of myeloid marker CpGs across histone modifications and DNAse hypersensitivity sites (DHS) identified in myeloid cells.

(E) Gene ontology processes and KEGG pathway enrichment analysis for myeloid marker CpGs.

(F) Distribution of myeloid marker CpGs per gene.

(G) Genome track depicting epigenomic features (H3K4me1 ChIP-Seq, DHS - Blueprint) of myeloid cells across the *ARID5B* loci. The location of n=6 myeloid marker CpGs that cluster at the *ARID5B* variant 2 transcription start site (TSS) is highlighted in red and magnified further below to show DNAm profiles (beta values) across each myeloid cell type and AMs. Lines indicate average DNAm across all of the CpGs assayed in the magnified region.

Figure 2:

(A) Heatmap depicting predicted myeloid cell composition of airway macrophages (AMs - columns) after deconvolution of DNA methylation (DNAm) profiles with myeloid maker-CpGs generated from reference monocyte and macrophage methylomes (rows).

(B) Difference in myeloid cell composition were evident for AMs derived from healthy and IPF donors for 'classical' and 'M1 macrophages' respectively. P-values determined by one-way ANOVA with Tukey's correction for multiple testing.

(C) Spearman-rank correlation between donor age and composition of AMs DNAm attributed to classical monocytes and M1 macrophages.

(D) Epigenetic clock analysis indicating a correlation between chronological and epigenetic age as determined by the Hannum et. al 'clock' (top). By comparing residuals from two age-adjusted epigenetic 'clocks' (Hannum and Horvath) it was determined IPF AMs exhibited no epigenetic age acceleration compared to AMs from healthy controls.

(E) Spearman-rank correlation between epigenetic age acceleration and composition of AMs DNAm attributed to classical monocytes and M1 macrophages.

Figure 3:

(A) Quantile-quantile plots depicting the impact of adjustment for myeloid cell composition in addition to other study covariates on identification of differentially methylated positions (DMPs) in IPF. Those DMPs reaching the epigenome-wide significance (EWAS) threshold of $P<9x10^{-8}$ are highlighted in red.

(B) Volcano plot depicting impact of myeloid cell-adjustment and direction of DNA methylation (DNAm) changes of DMPs in IPF. Dashed line represents EWAS P-value threshold.

(C) Genome track depicting epigenomic features (H3K4me1 ChIP-Seq, DNase-I hypersensitivity - DHS - Blueprint) of myeloid cells across the *LPCAT1* loci. Regions interacting with the *LPCAT1* promoter in 3D as determined by promoter-capture HiC (pcHiC) are indicated in grey. Interactions with frequency threshold >5 in myeloid

cells are highlighted in purple. The location of n=3 intronic IPF DMPs are highlighted in red and magnified further below to show methylation profiles (beta values) of healthy and IPF AMs across the respective CpGs (*). Lines indicate average methylation across all of the CpGs assayed in the magnified region.

(D) Relationship between DNAm of IPF DMPs and gene expression for *LPCAT1* across Healthy (blue) and IPF (red) donor AMs.

(E-F) Relationship between gene expression (E), methylation of an IPF-associated DMP (F) for *LPCAT1* and forced vital capacity (FVC).

Figure 4:

(A) Volcano plot depicting impact of myeloid cell-adjustment and direction of DNA methylation (DNAm) changes of differentially methylated regions (DMRs) in IPF.

(B) Genomic feature distribution for all EPIC array CpGs and those encompassed by IPF DMRs.

(C-D) Enrichment of IPF DMRs across histone modifications and DNAse-I hypersensitivity sites (DHS) in monocytes and macrophages.

(E) DNA motif enrichment in IPF DMRs.

Figure 5:

(A) Network depicting protein-protein interactions of DMRs-associated genes.

(B) Gene ontology processes and KEGG pathway enrichment analysis for DMR-associated genes gaining or losing DNA methylation (DNAm) in IPF.

(C) Genome track depicting epigenomic features (H3K4me1 ChIP-Seq, DNase hypersensitivity - DHS - Blueprint) of myeloid cells across the *PFKFB3* loci. The location of the IPF DMR is highlighted in red and magnified further below to show

596 methylation profiles (beta values) at the associated n=3 CpGs (*) across healthy and
597 IPF AMs. Lines indicate average methylation across all of the CpGs assayed in the
598 magnified region.
599 (D) Relationship between DNAm of IPF DMPs and gene expression for *PFKFB3*
600 across Healthy (blue) and IPF (red) donor AMs.
601 (E-F) Relationship between gene expression (E), methylation of DMR-associated
602 CpG (F) for *PFKFB3* and forced vital capacity (FVC).
603

604 **Figure S1**

605 (A) Heatmap depicting DNA methylation (DNAm) profiles across myeloid cells (i.e.
606 monocytes and M0, M1, M2 macrophages) and AMs from healthy and IPF donors for
607 genes containing >2 myeloid marker CpGs (Table S2).
608 (B) Disease origin and cell-type expression of genes highlighted in this study in
609 single cell RNA-Seq data from the IPF lung. Gene expression is projected over
610 UMAP representation of all disease/cell-types with brighter colours indicating more
611 expression. Full data available at www.ipfcellatlas.com.
612 (C) Gene expression of genes highlight in this study in AMs from healthy and IPF
613 donors as determined by qPCR. * P<0.05, ** P<0.05 Mann-Whitey Test.
614 (D) Spearman-rank correlations for chronological and epigenetic age (right) and for
615 epigenetic age acceleration and composition of AMs DNAm attributed to classical
616 monocytes and M1 macrophages (left) as determined by the Horvath et. al 'clock'.
617

618 **Figure S2**

619 (A) PCA plot of normalized DNA methylation (DNAm) data for all CpGs prior to
620 differential analysis indicating separation of healthy and IPF AMs.

(B) Sources of variation in DNAm dataset across the first 5 principal components for all CpGs. Associated P values were generated through RnBeads pipline.

(C-D) Plots depicting changes in DNAm (beta value) for healthy and IPF donors across Intronic (C) and intergenic (D) DMPs (Table S3).

(E) Enrichment of IPF differentially methylated positions (DMPs) across DNAse hypersensitivity sites (DHS) in monocytes and macrophages.

(F) All regions interacting with the *LPCAT1* promoter in 3D as determined by promoter-capture HiC (pcHiC). In addition to self-interacting with the region containing IPF DMPs (purple, Figure 2E), *LPCAT1* additionally interacts with the promoters of *SLC6A3* and *SLC12A7*. Dashed line indicates interactions with frequency threshold >5.

(G) Relationship between DNAm of IPF DMPs and gene expression for *SLC6A3* across Healthy (blue) and IPF (red) donor AMs. No *SLC12A7* gene expression was detected in AMs.

Figure S3:

(A) Proportion of unique promoter-capture HiC (pcHiC) 'other ends' containing any EPIC CpGs or those identified as differentially methylated positions (DMPs) or DMRs in IPF.

(B) Proportion of all EPIC, DMPs and DMRs that are linked in 3D as determined by pcHiC. **** P<0.0001, Chi-square test with Yates correction versus all interactions containing EPIC CpGs.

(C) Number of 3D interactions per IPF DMRs (Table S4).

(D) Cell-type expression of transcription factor genes with enriched motifs in IPF DMRs in single cell RNA-Seq data from the IPF lung. Gene expression is projected

646 over UMAP representation of all cell-types with brighter colours indicating more
647 expression. Full data available at www.ipfcellatlas.com.
648
649 **Figure S4:**
650 (A-B) Gene ontology processes and KEGG pathway enrichment analysis for all
651 DMR-associated genes (A) and all those forming protein-protein interactions
652 regardless of DNAm status in IPF (B).

References

1 Byrne, A. J., Maher, T. M. & Lloyd, C. M. Pulmonary Macrophages: A New Therapeutic Pathway in Fibrosing Lung Disease? *Trends in Molecular Medicine* **22**, 303-316, doi:https://doi.org/10.1016/j.molmed.2016.02.004 (2016).

2 Misharin, A. V. *et al.* Monocyte-derived alveolar macrophages drive lung fibrosis and persist in the lung over the life span. *J Exp Med* **214**, 2387-2404, doi:10.1084/jem.20162152 (2017).

3 Byrne, A. J. *et al.* Dynamics of human monocytes and airway macrophages during healthy aging and after transplant. *The Journal of Experimental Medicine* **217**, doi:10.1084/jem.20191236 (2020).

4 Lavin, Y. *et al.* Tissue-Resident Macrophage Enhancer Landscapes Are Shaped by the Local Microenvironment. *Cell* **159**, 1312-1326, doi:https://doi.org/10.1016/j.cell.2014.11.018 (2014).

5 Adams, T. S. *et al.* Single-cell RNA-seq reveals ectopic and aberrant lung-resident cell populations in idiopathic pulmonary fibrosis. *Science Advances* **6**, eaba1983, doi:10.1126/sciadv.aba1983 (2020).

6 Habermann, A. C. *et al.* Single-cell RNA sequencing reveals profibrotic roles of distinct epithelial and mesenchymal lineages in pulmonary fibrosis. *Science Advances* **6**, eaba1972, doi:10.1126/sciadv.aba1972 (2020).

7 Reyfman, P. A. *et al.* Single-Cell Transcriptomic Analysis of Human Lung Provides Insights into the Pathobiology of Pulmonary Fibrosis. *American Journal of Respiratory and Critical Care Medicine* **199**, 1517-1536, doi:10.1164/rccm.201712-2410OC (2018).

8 Wallner, S. *et al.* Epigenetic dynamics of monocyte-to-macrophage differentiation. *Epigenetics & Chromatin* **9**, 33, doi:10.1186/s13072-016-0079-z (2016).

9 Tirado-Magallanes, R., Rebbani, K., Lim, R., Pradhan, S. & Benoukraf, T. Whole genome DNA methylation: beyond genes silencing. *Oncotarget* **8**, 5629-5637, doi:10.18632/oncotarget.13562 (2017).

10 Schübeler, D. Function and information content of DNA methylation. *Nature* **517**, 321-326, doi:10.1038/nature14192 (2015).

11 Chen, Y. *et al.* Genome-wide DNA methylation profiling shows a distinct epigenetic signature associated with lung macrophages in cystic fibrosis. *Clinical epigenetics* **10**, 152-152, doi:10.1186/s13148-018-0580-2 (2018).

12 Fricker, M. & Gibson, P. G. Macrophage dysfunction in the pathogenesis and treatment of asthma. *European Respiratory Journal* **50**, 1700196, doi:10.1183/13993003.00196-2017 (2017).

13 He, L.-X., Tang, Z.-H., Huang, Q.-S. & Li, W.-H. DNA Methylation: A Potential Biomarker of Chronic Obstructive Pulmonary Disease. *Frontiers in cell and developmental biology* **8**, 585-585, doi:10.3389/fcell.2020.00585 (2020).

14 Armstrong, D. A. *et al.* DNA Methylation Changes in Regional Lung Macrophages Are Associated with Metabolic Differences. *ImmunoHorizons* **3**, 274, doi:10.4049/immunohorizons.1900042 (2019).

15 Martinez, F. J. *et al.* Idiopathic pulmonary fibrosis. *Nature Reviews Disease Primers* **3**, 17074, doi:10.1038/nrdp.2017.74 (2017).

16 Chambers, R. C. & Mercer, P. F. Mechanisms of alveolar epithelial injury, repair, and fibrosis. *Annals of the American Thoracic Society* **12 Suppl 1**, S16-S20, doi:10.1513/AnnalsATS.201410-448MG (2015).

17 Allen, R. J. *et al.* Genome-Wide Association Study of Susceptibility to Idiopathic Pulmonary Fibrosis. *Am J Respir Crit Care Med* **201**, 564-574, doi:10.1164/rccm.201905-1017OC (2020).

18 Molyneaux, P. L. *et al.* Host–Microbial Interactions in Idiopathic Pulmonary Fibrosis. *American Journal of Respiratory and Critical Care Medicine* **195**, 1640-1650, doi:10.1164/rccm.201607-1408OC (2017).

19 Vancheri, C., Failla, M., Crimi, N. & Raghu, G. Idiopathic pulmonary fibrosis: a disease with similarities and links to cancer biology. *European Respiratory Journal* **35**, 496, doi:10.1183/09031936.00077309 (2010).

20 Allden, S. J. *et al.* The Transferrin Receptor CD71 Delineates Functionally Distinct Airway Macrophage Subsets during Idiopathic Pulmonary Fibrosis. *American Journal of Respiratory and Critical Care Medicine* **200**, 209-219, doi:10.1164/rccm.201809-1775OC (2019).

21 Ogger, P. P. *et al.* Itaconate controls the severity of pulmonary fibrosis. *Science Immunology* **5**, eabc1884, doi:10.1126/sciimmunol.abc1884 (2020).

718 22 Pidsley, R. *et al.* Critical evaluation of the Illumina MethylationEPIC BeadChip
719 microarray for whole-genome DNA methylation profiling. *Genome Biol* **17**,
720 208, doi:10.1186/s13059-016-1066-1 (2016).
721 23 Stunnenberg, H. G. & Hirst, M. The International Human Epigenome
722 Consortium: A Blueprint for Scientific Collaboration and Discovery. *Cell* **167**,
723 1145-1149, doi:10.1016/j.cell.2016.11.007 (2016).
724 24 Okazaki, Y. *et al.* Increased glucose metabolism in Arid5b−/− skeletal muscle
725 is associated with the down-regulation of TBC1 domain family member 1
726 (TBC1D1). *Biological Research* **53**, 45, doi:10.1186/s40659-020-00313-3
727 (2020).
728 25 Du, Y. *et al.* Lysophosphatidylcholine acyltransferase 1 upregulation and
729 concomitant phospholipid alterations in clear cell renal cell carcinoma. *J Exp*
730 *Clin Cancer Res* **36**, 66, doi:10.1186/s13046-017-0525-1 (2017).
731 26 Javierre, B. M. *et al.* Lineage-Specific Genome Architecture Links Enhancers
732 and Non-coding Disease Variants to Target Gene Promoters. *Cell* **167**, 1369-
733 1384.e1319, doi:10.1016/j.cell.2016.09.037 (2016).
734 27 Richeldi, L. *et al.* Relative versus absolute change in forced vital capacity in
735 idiopathic pulmonary fibrosis. *Thorax* **67**, 407, doi:10.1136/thoraxjnl-2011-
736 201184 (2012).
737 28 Finucane, O. M., Sugrue, J., Rubio-Araiz, A., Guillot-Sestier, M. V. & Lynch,
738 M. A. The NLRP3 inflammasome modulates glycolysis by increasing PFKFB3
739 in an IL-1β-dependent manner in macrophages. *Sci Rep* **9**, 4034,
740 doi:10.1038/s41598-019-40619-1 (2019).
741 29 Herazo-Maya, J. D. *et al.* Validation of a 52-gene risk profile for outcome
742 prediction in patients with idiopathic pulmonary fibrosis: an international,
743 multicentre, cohort study. *The Lancet Respiratory Medicine* **5**, 857-868,
744 doi:https://doi.org/10.1016/S2213-2600(17)30349-1 (2017).
745 30 Herazo-Maya, J. D. *et al.* Peripheral Blood Mononuclear Cell Gene
746 Expression Profiles Predict Poor Outcome in Idiopathic Pulmonary Fibrosis.
747 *Science Translational Medicine* **5**, 205ra136,
748 doi:10.1126/scitranslmed.3005964 (2013).
749 31 Scott, M. K. D. *et al.* Increased monocyte count as a cellular biomarker for
750 poor outcomes in fibrotic diseases: a retrospective, multicentre cohort study.

The Lancet Respiratory Medicine **7**, 497-508, doi:10.1016/S2213-2600(18)30508-3 (2019).

32 Titus, A. J., Gallimore, R. M., Salas, L. A. & Christensen, B. C. Cell-type deconvolution from DNA methylation: a review of recent applications. *Human molecular genetics* **26**, R216-R224, doi:10.1093/hmg/ddx275 (2017).

33 Yang, I. V. *et al.* Relationship of DNA Methylation and Gene Expression in Idiopathic Pulmonary Fibrosis. *American Journal of Respiratory and Critical Care Medicine* **190**, 1263-1272, doi:10.1164/rccm.201408-1452OC (2014).

34 Sanders, Y. Y. *et al.* Altered DNA Methylation Profile in Idiopathic Pulmonary Fibrosis. *American Journal of Respiratory and Critical Care Medicine* **186**, 525-535, doi:10.1164/rccm.201201-0077OC (2012).

35 Yang, I. V. & Schwartz, D. A. Epigenetics of idiopathic pulmonary fibrosis. *Translational research : the journal of laboratory and clinical medicine* **165**, 48-60, doi:10.1016/j.trsl.2014.03.011 (2015).

36 Bell, C. G. *et al.* DNA methylation aging clocks: challenges and recommendations. *Genome Biology* **20**, 249, doi:10.1186/s13059-019-1824-y (2019).

37 Horvath, S. & Raj, K. DNA methylation-based biomarkers and the epigenetic clock theory of ageing. *Nature Reviews Genetics* **19**, 371-384, doi:10.1038/s41576-018-0004-3 (2018).

38 Shchukina, I. *et al.* Epigenetic aging of classical monocytes from healthy individuals. *bioRxiv*, 2020.2005.2010.087023, doi:10.1101/2020.05.10.087023 (2020).

39 Corces, M. R. *et al.* Lineage-specific and single-cell chromatin accessibility charts human hematopoiesis and leukemia evolution. *Nature Genetics* **48**, 1193-1203, doi:10.1038/ng.3646 (2016).

40 Okuno, Y., Inoue, K. & Imai, Y. Novel insights into histone modifiers in adipogenesis. *Adipocyte* **2**, 285-288, doi:10.4161/adip.25731 (2013).

41 Claussnitzer, M. *et al.* FTO Obesity Variant Circuitry and Adipocyte Browning in Humans. *New England Journal of Medicine* **373**, 895-907, doi:10.1056/NEJMoa1502214 (2015).

42 Baba, A. *et al.* PKA-dependent regulation of the histone lysine demethylase complex PHF2–ARID5B. *Nature Cell Biology* **13**, 668-675, doi:10.1038/ncb2228 (2011).

43 Cichocki, F. *et al.* ARID5B regulates metabolic programming in human adaptive NK cells. *The Journal of experimental medicine* **215**, 2379-2395, doi:10.1084/jem.20172168 (2018).

44 Liu, Y. *et al.* Blood monocyte transcriptome and epigenome analyses reveal loci associated with human atherosclerosis. *Nature Communications* **8**, 393, doi:10.1038/s41467-017-00517-4 (2017).

45 Chen, X., Hyatt, B. A., Mucenski, M. L., Mason, R. J. & Shannon, J. M. Identification and characterization of a lysophosphatidylcholine acyltransferase in alveolar type II cells. *Proc Natl Acad Sci U S A* **103**, 11724-11729, doi:10.1073/pnas.0604946103 (2006).

46 Bridges, J. P. *et al.* LPCAT1 regulates surfactant phospholipid synthesis and is required for transitioning to air breathing in mice. *The Journal of Clinical Investigation* **120**, 1736-1748, doi:10.1172/JCI38061 (2010).

47 Bi, J. *et al.* Oncogene Amplification in Growth Factor Signaling Pathways Renders Cancers Dependent on Membrane Lipid Remodeling. *Cell Metabolism* **30**, 525-538.e528, doi:https://doi.org/10.1016/j.cmet.2019.06.014 (2019).

48 Xu, Y. *et al.* Single-cell RNA sequencing identifies diverse roles of epithelial cells in idiopathic pulmonary fibrosis. *JCI Insight* **1**, doi:10.1172/jci.insight.90558 (2017).

49 Leslie, J. *et al.* c-Rel orchestrates energy-dependent epithelial and macrophage reprogramming in fibrosis. *Nature Metabolism*, doi:10.1038/s42255-020-00306-2 (2020).

50 Tawakol, A. *et al.* HIF-1α and PFKFB3 Mediate a Tight Relationship Between Proinflammatory Activation and Anerobic Metabolism in Atherosclerotic Macrophages. *Arteriosclerosis, thrombosis, and vascular biology* **35**, 1463-1471, doi:10.1161/ATVBAHA.115.305551 (2015).

51 Müller, F. *et al.* RnBeads 2.0: comprehensive analysis of DNA methylation data. *Genome Biol* **20**, 55, doi:10.1186/s13059-019-1664-9 (2019).

52 Zhou, W., Laird, P. W. & Shen, H. Comprehensive characterization, annotation and innovative use of Infinium DNA methylation BeadChip probes. *Nucleic Acids Research* **45**, e22-e22, doi:10.1093/nar/gkw967 (2016).

53 Pidsley, R. *et al.* A data-driven approach to preprocessing Illumina 450K methylation array data. *BMC Genomics* **14**, 293, doi:10.1186/1471-2164-14-293 (2013).

54 Houseman, E. A. *et al.* Reference-free deconvolution of DNA methylation data and mediation by cell composition effects. *BMC Bioinformatics* **17**, 259, doi:10.1186/s12859-016-1140-4 (2016).

55 Min, J. L., Hemani, G., Davey Smith, G., Relton, C. & Suderman, M. Meffil: efficient normalization and analysis of very large DNA methylation datasets. *Bioinformatics* **34**, 3983-3989, doi:10.1093/bioinformatics/bty476 (2018).

56 Mansell, G. *et al.* Guidance for DNA methylation studies: statistical insights from the Illumina EPIC array. *BMC Genomics* **20**, 366, doi:10.1186/s12864-019-5761-7 (2019).

57 Peters, T. J. *et al.* De novo identification of differentially methylated regions in the human genome. *Epigenetics Chromatin* **8**, 6, doi:10.1186/1756-8935-8-6 (2015).

58 Heinz, S. *et al.* Simple combinations of lineage-determining transcription factors prime cis-regulatory elements required for macrophage and B cell identities. *Mol Cell* **38**, 576-589, doi:10.1016/j.molcel.2010.05.004 (2010).

59 Breeze, C. E. *et al.* eFORGE v2.0: updated analysis of cell type-specific signal in epigenomic data. *Bioinformatics* **35**, 4767-4769, doi:10.1093/bioinformatics/btz456 (2019).

60 Pageaud, Y., Plass, C. & Assenov, Y. Enrichment analysis with EpiAnnotator. *Bioinformatics* **34**, 1781-1783, doi:10.1093/bioinformatics/bty007 (2018).

61 Afgan, E. *et al.* The Galaxy platform for accessible, reproducible and collaborative biomedical analyses: 2016 update. *Nucleic Acids Research* **44**, W3-W10, doi:10.1093/nar/gkw343 (2016).

62 Oki, S. *et al.* ChIP-Atlas: a data-mining suite powered by full integration of public ChIP-seq data. *EMBO reports* **19**, e46255, doi:10.15252/embr.201846255 (2018).

63 Zhou, G. *et al.* NetworkAnalyst 3.0: a visual analytics platform for comprehensive gene expression profiling and meta-analysis. *Nucleic Acids Res* **47**, W234-W241, doi:10.1093/nar/gkz240 (2019).

64 Aryee, M. J. *et al.* Minfi: a flexible and comprehensive Bioconductor package for the analysis of Infinium DNA methylation microarrays. *Bioinformatics (Oxford, England)* **30**, 1363-1369, doi:10.1093/bioinformatics/btu049 (2014).

65 Horvath, S. DNA methylation age of human tissues and cell types. *Genome Biology* **14**, 3156, doi:10.1186/gb-2013-14-10-r115 (2013).

66 Hannum, G. *et al.* Genome-wide methylation profiles reveal quantitative views of human aging rates. *Mol Cell* **49**, 359-367, doi:10.1016/j.molcel.2012.10.016 (2013).

67 Kulakovskiy, I. V. *et al.* HOCOMOCO: expansion and enhancement of the collection of transcription factor binding sites models. *Nucleic Acids Research* **44**, D116-D125, doi:10.1093/nar/gkv1249 (2016).

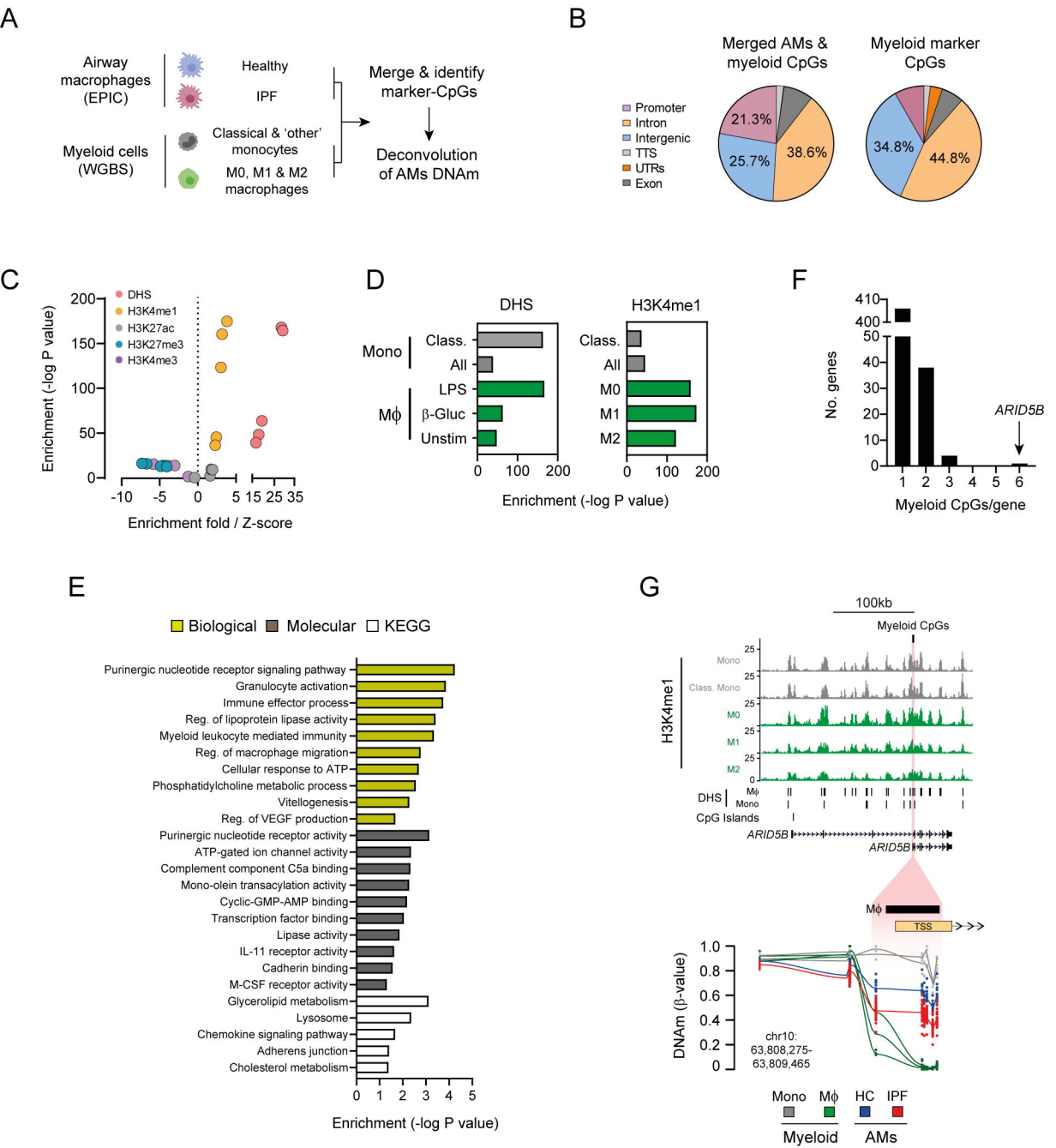
A
Airway macrophages (EPIC)
Healthy
IPF
Myeloid cells (WGBS)
Classical & 'other' monocytes
M0, M1 & M2 macrophages
Merge & identify marker-CpGs
Deconvolution of AMs DNAm
B
Merged AMs & myeloid CpGs
Myeloid marker CpGs
Promoter
Intron
Intergenic
TTS
UTRs
Exon
21.3%
25.7%
38.6%
34.8%
44.8%
C
DHS
H3K4me1
H3K27ac
H3K27me3
H3K4me3
Enrichment (-log P value)
Enrichment fold / Z-score
D
DHS
H3K4me1
Mono
Mϕ
Class.
All
LPS
β-Gluc
Unstim
M0
M1
M2
Enrichment (-log P value)
F
No. genes
ARID5B
Myeloid CpGs/gene
E
Biological
Molecular
KEGG
Purinergic nucleotide receptor signaling pathway
Granulocyte activation
Immune effector process
Reg. of lipoprotein lipase activity
Myeloid leukocyte mediated immunity
Reg. of macrophage migration
Cellular response to ATP
Phosphatidylcholine metabolic process
Vitellogenesis
Reg. of VEGF production
Purinergic nucleotide receptor activity
ATP-gated ion channel activity
Complement component C5a binding
Mono-olein transacylation activity
Cyclic-GMP-AMP binding
Transcription factor binding
Lipase activity
IL-11 receptor activity
Cadherin binding
M-CSF receptor activity
Glycerolipid metabolism
Lysosome
Chemokine signaling pathway
Adherens junction
Cholesterol metabolism
Enrichment (-log P value)
G
100kb
Myeloid CpGs
H3K4me1
Mono
Class. Mono
M0
M1
M2
DHS
CpG Islands
ARID5B
TSS
DNAm (β-value)
chr10:
63,808,275-
63,809,465
Mono
HC
IPF
Myeloid
AMs

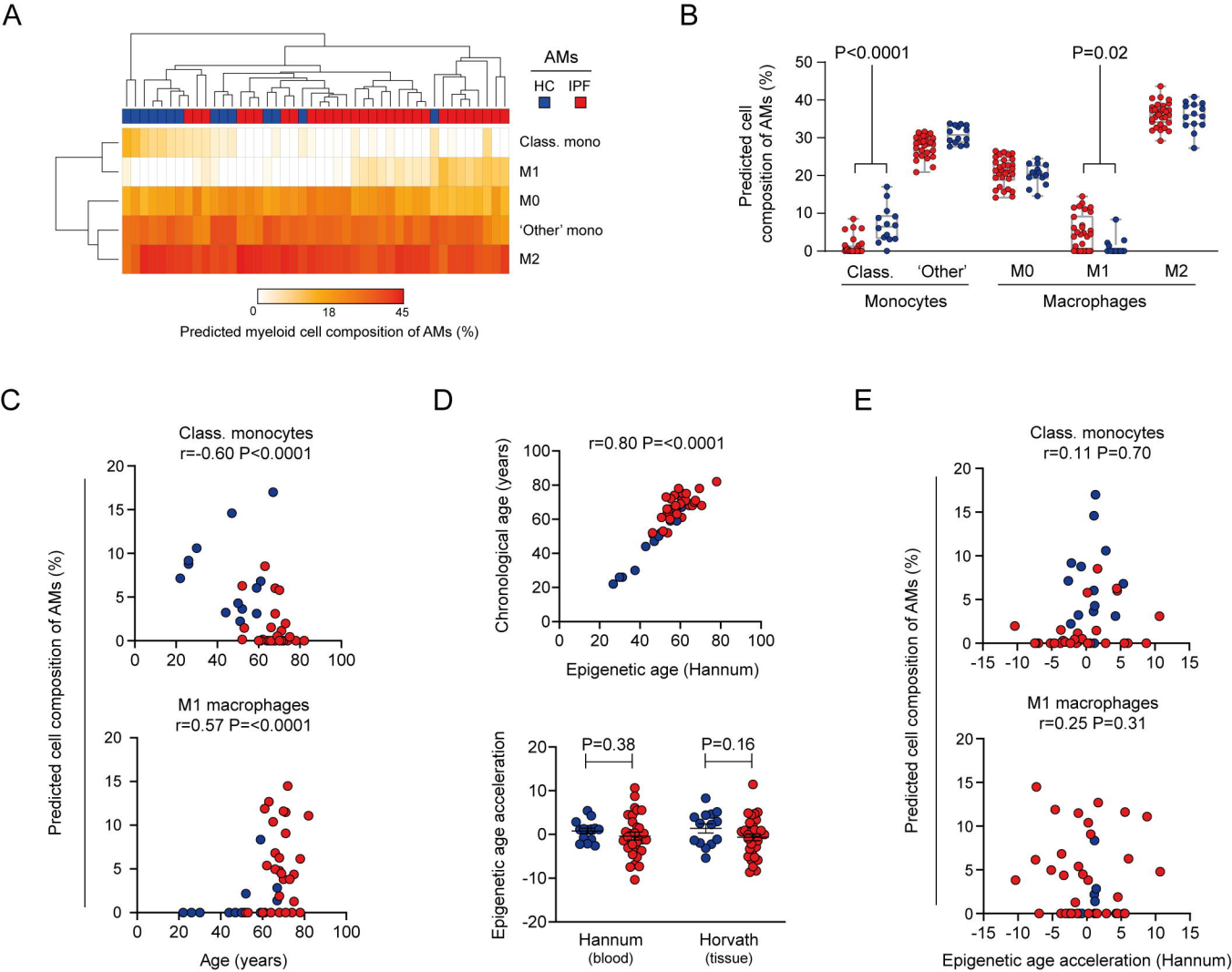
A
AMs
HC
IPF
Class. mono
M1
M0
'Other' mono
M2
0
18
45
Predicted myeloid cell composition of AMs (%)
B
P<0.0001
P=0.02
Predicted cell composition of AMs (%)
Class.
'Other'
M0
M1
M2
Monocytes
Macrophages
C
Class. monocytes
r=-0.60 P<0.0001
M1 macrophages
r=0.57 P=<0.0001
Predicted cell composition of AMs (%)
Age (years)
D
r=0.80 P=<0.0001
Chronological age (years)
Epigenetic age (Hannum)
P=0.38
P=0.16
Epigenetic age acceleration
Hannum
(blood)
Horvath
(tissue)
E
Class. monocytes
r=0.11 P=0.70
M1 macrophages
r=0.25 P=0.31
Predicted cell composition of AMs (%)
Epigenetic age acceleration (Hannum)

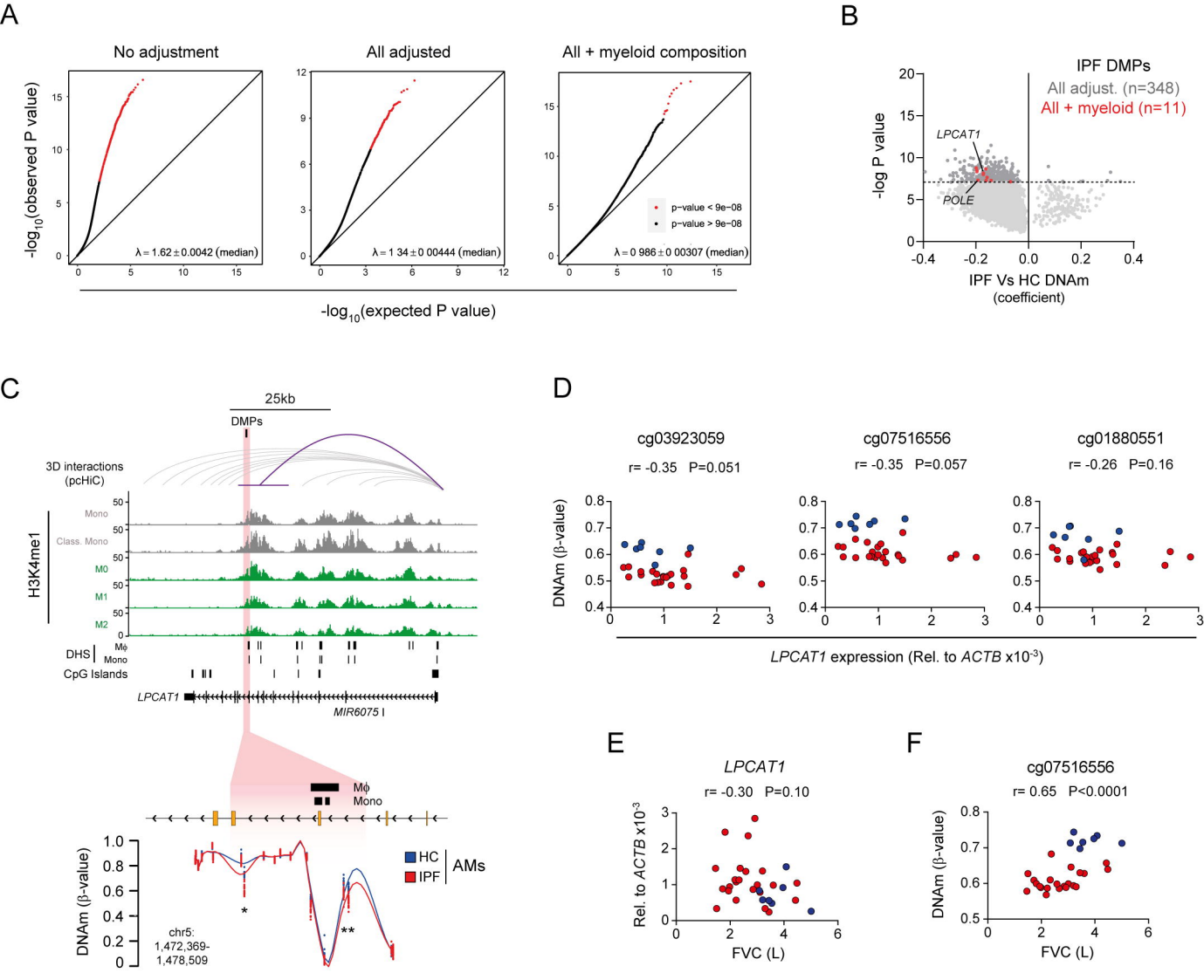
A
No adjustment
All adjusted
All + myeloid composition
-log10(observed P value)
-log10(expected P value)
λ = 1.62 ± 0.0042 (median)
λ = 1 34 ± 0 00444 (median)
λ = 0 986 ± 0 00307 (median)
p-value < 9e-08
p-value > 9e-08
B
IPF DMPs
All adjust. (n=348)
All + myeloid (n=11)
LPCAT1
POLE
-log P value
IPF Vs HC DNAm
(coefficient)
C
25kb
DMPs
3D interactions
(pcHiC)
H3K4me1
Mono
Class. Mono
M0
M1
M2
DHS
Mϕ
Mono
CpG Islands
LPCAT1
MIR6075
Mϕ
Mono
HC
IPF
AMs
DNAm (β-value)
chr5:
1,472,369-
1,478,509
D
cg03923059
r= -0.35 P=0.051
cg07516556
r= -0.35 P=0.057
cg01880551
r= -0.26 P=0.16
DNAm (β-value)
LPCAT1 expression (Rel. to ACTB x10-3)
E
LPCAT1
r= -0.30 P=0.10
Rel. to ACTB x10-3
FVC (L)
F
cg07516556
r= 0.65 P<0.0001
DNAm (β-value)
FVC (L)

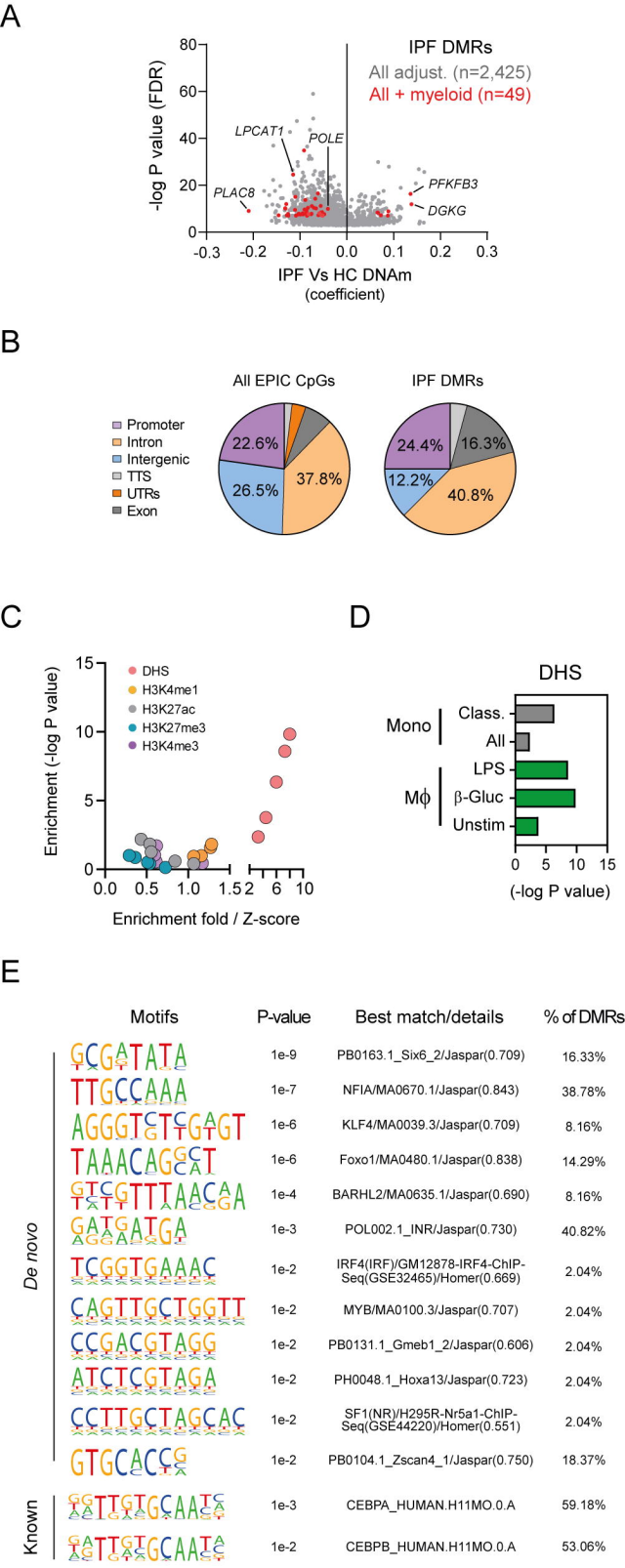
A
IPF DMRs
All adjust. (n=2,425)
All + myeloid (n=49)
-log P value (FDR)
LPCAT1
POLE
PLAC8
PFKFB3
DGKG
IPF Vs HC DNAm
(coefficient)
B
All EPIC CpGs
IPF DMRs
Promoter
Intron
Intergenic
TTS
UTRs
Exon
22.6%
37.8%
26.5%
24.4%
16.3%
12.2%
40.8%
C
DHS
H3K4me1
H3K27ac
H3K27me3
H3K4me3
Enrichment (-log P value)
Enrichment fold / Z-score
D
DHS
Mono
Class.
All
Mϕ
LPS
β-Gluc
Unstim
(-log P value)
E
Motifs
P-value
Best match/details
% of DMRs
De novo
1e-9
PB0163.1_Six6_2/Jaspar(0.709)
16.33%
1e-7
NFIA/MA0670.1/Jaspar(0.843)
38.78%
1e-6
KLF4/MA0039.3/Jaspar(0.709)
8.16%
1e-6
Foxo1/MA0480.1/Jaspar(0.838)
14.29%
1e-4
BARHL2/MA0635.1/Jaspar(0.690)
8.16%
1e-3
POL002.1_INR/Jaspar(0.730)
40.82%
1e-2
IRF4(IRF)/GM12878-IRF4-ChIP-Seq(GSE32465)/Homer(0.669)
2.04%
1e-2
MYB/MA0100.3/Jaspar(0.707)
2.04%
1e-2
PB0131.1_Gmeb1_2/Jaspar(0.606)
2.04%
1e-2
PH0048.1_Hoxa13/Jaspar(0.723)
2.04%
1e-2
SF1(NR)/H295R-Nr5a1-ChIP-Seq(GSE44220)/Homer(0.551)
2.04%
1e-2
PB0104.1_Zscan4_1/Jaspar(0.750)
18.37%
Known
1e-3
CEBPA_HUMAN.H11MO.0.A
59.18%
1e-2
CEBPB_HUMAN.H11MO.0.A
53.06%

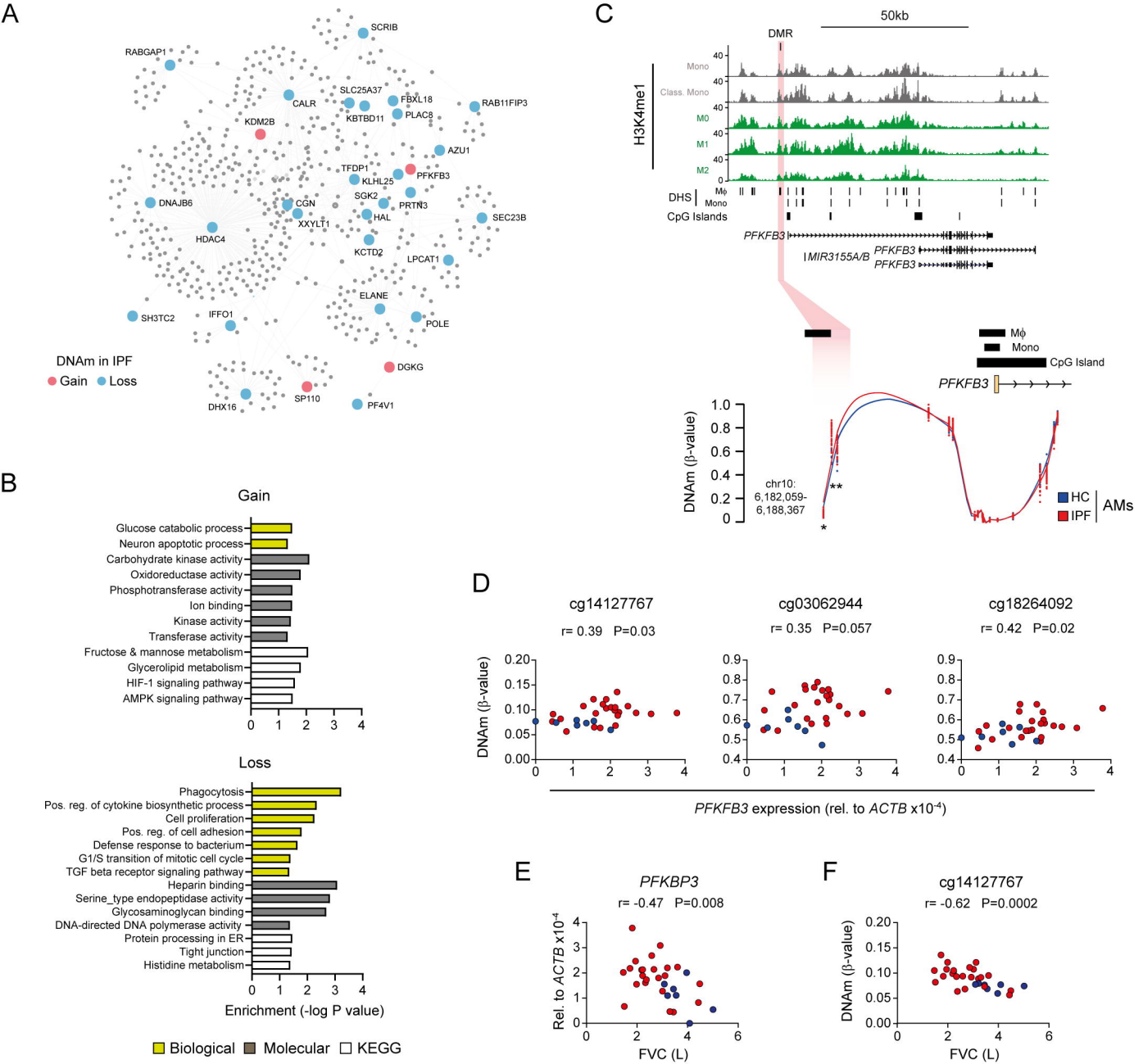
A
SCRIB
RABGAP1
SLC25A37
CALR
FBXL18
RAB11FIP3
KBTBD11
PLAC8
KDM2B
AZU1
TFDP1
PFKFB3
KLHL25
DNAJB6
CGN
SGK2
PRTN3
HAL
SEC23B
XXYLT1
HDAC4
KCTD2
LPCAT1
ELANE
SH3TC2
IFFO1
POLE
DGKG
DHX16
SP110
PF4V1
DNAm in IPF
Gain
Loss
B
Gain
Glucose catabolic process
Neuron apoptotic process
Carbohydrate kinase activity
Oxidoreductase activity
Phosphotransferase activity
Ion binding
Kinase activity
Transferase activity
Fructose & mannose metabolism
Glycerolipid metabolism
HIF-1 signaling pathway
AMPK signaling pathway
0 1 2 3 4
Loss
Phagocytosis
Pos. reg. of cytokine biosynthetic process
Cell proliferation
Pos. reg. of cell adhesion
Defense response to bacterium
G1/S transition of mitotic cell cycle
TGF beta receptor signaling pathway
Heparin binding
Serine_type endopeptidase activity
Glycosaminoglycan binding
DNA-directed DNA polymerase activity
Protein processing in ER
Tight junction
Histidine metabolism
0 1 2 3 4
Enrichment (-log P value)
Biological
Molecular
KEGG
C
50kb
DMR
H3K4me1
Mono
Class. Mono
M0
M1
M2
DHS
Mϕ
Mono
CpG Islands
PFKFB3
MIR3155A/B
PFKFB3
PFKFB3
Mϕ
Mono
CpG Island
PFKFB3
DNAm (β-value)
1.0
0.8
0.6
0.4
0.2
0
chr10:
6,182,059-
6,188,367
**
*
HC
IPF
AMs
D
cg14127767
r= 0.39 P=0.03
cg03062944
r= 0.35 P=0.057
cg18264092
r= 0.42 P=0.02
DNAm (β-value)
PFKFB3 expression (rel. to ACTB x10-4)
E
PFKBP3
r= -0.47 P=0.008
Rel. to ACTB x10-4
FVC (L)
F
cg14127767
r= -0.62 P=0.0002
DNAm (β-value)
FVC (L)